Supplementary Information (SI) for Environmental Science: Nano.

ELECTRONIC SUPPLEMENTARY INFORMATION

Unravelling the effect of non-metal doping on polymeric carbon nitride for enhanced degradation of broad-spectrum antibiotics under visible light

Debanjali Dey[a], Shamik Chowdhury[b]*, Ramkrishna Sen[a]*

[a]Department of Bioscience and Biotechnology,
Indian Institute of Technology Kharagpur, West Bengal 721302, India

[b]School of Environmental Science and Engineering,
Indian Institute of Technology Kharagpur, West Bengal 721302, India

*Corresponding author.

E-mail address: shamikc@iitkgp.ac.in (S. Chowdhury); rksen@bt.iitkgp.ac.in (R. Sen)

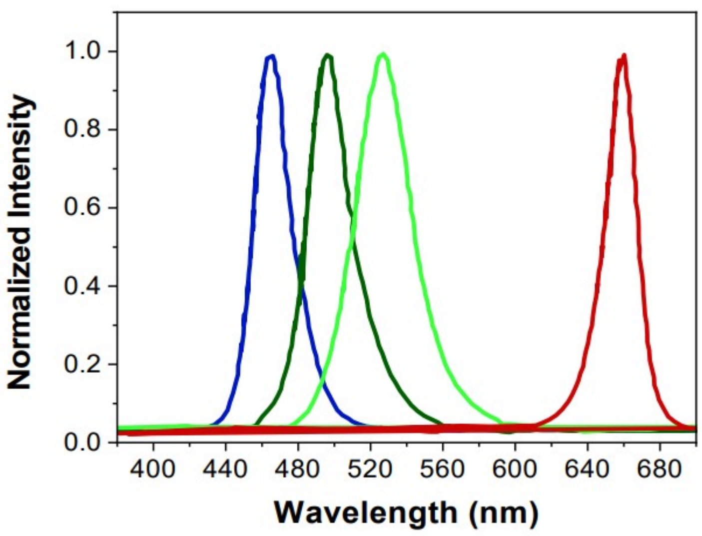

Fig. S1. Spectral distribution of the 250 W high-pressure mercury lamp, fitted with UV cutoff filter (λ < 420 nm), as provided by the manufacturer (Lelesil Innovative Systems, India).

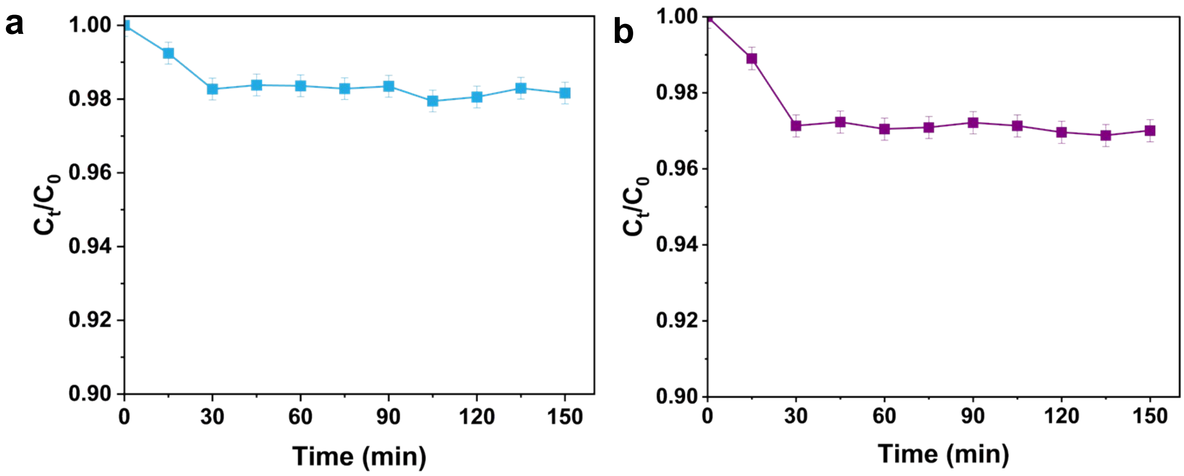

Fig. S2. Removal of (a) OFC and (b) SMZ by F-GCN without visible light illumination (experimental conditions: C_0 = 10 mg L^{-1}; photocatalyst dose = 1 g L^{-1}; temperature = 25 ± 2 °C)

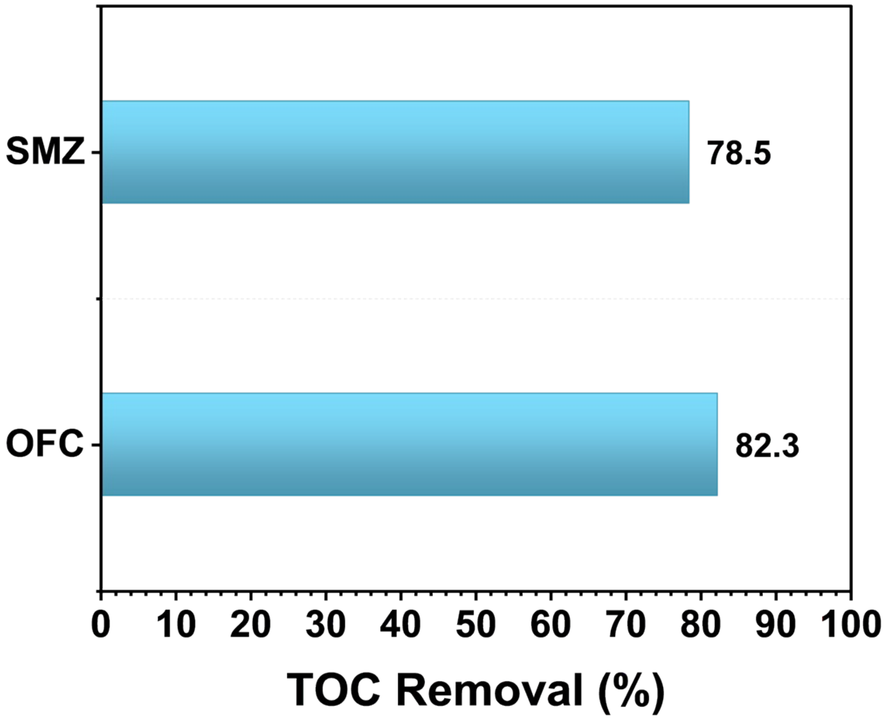

Fig. S3. TOC removal (%) during the photocatalytic degradation of OFC and SMZ over F-GCN.

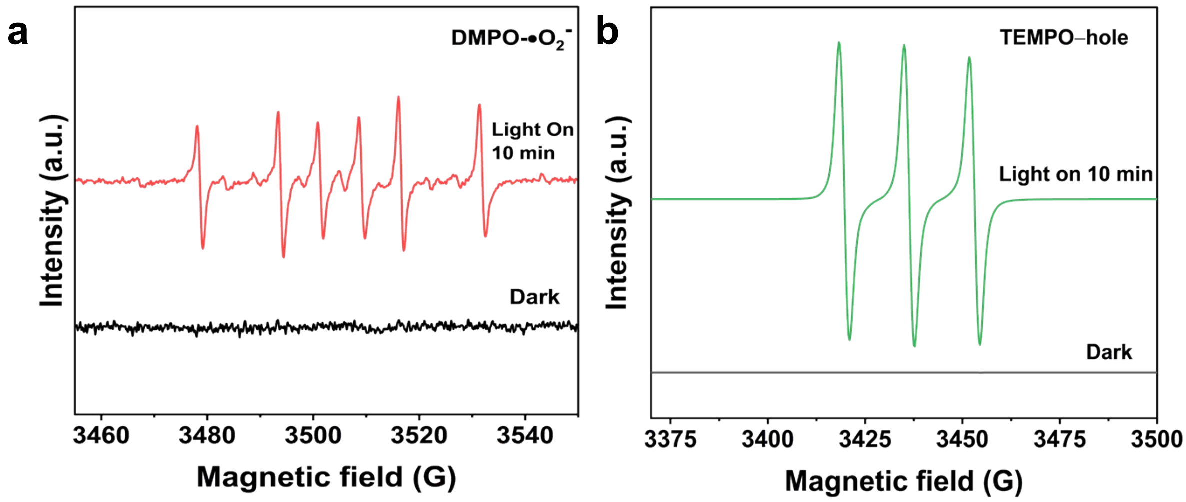

Fig. S4. EPR spectra showing radical adducts formed in F-GCN dispersions under visible-light irradiation, detected using spin-trapping agents: (a) DMPO-●O_2^- in methanol, (b) TEMPO–hole in aqueous solution (experimental conditions: F-GCN = 4 mg mL^{-1}, DMPO/TEMPO = 100 mM).

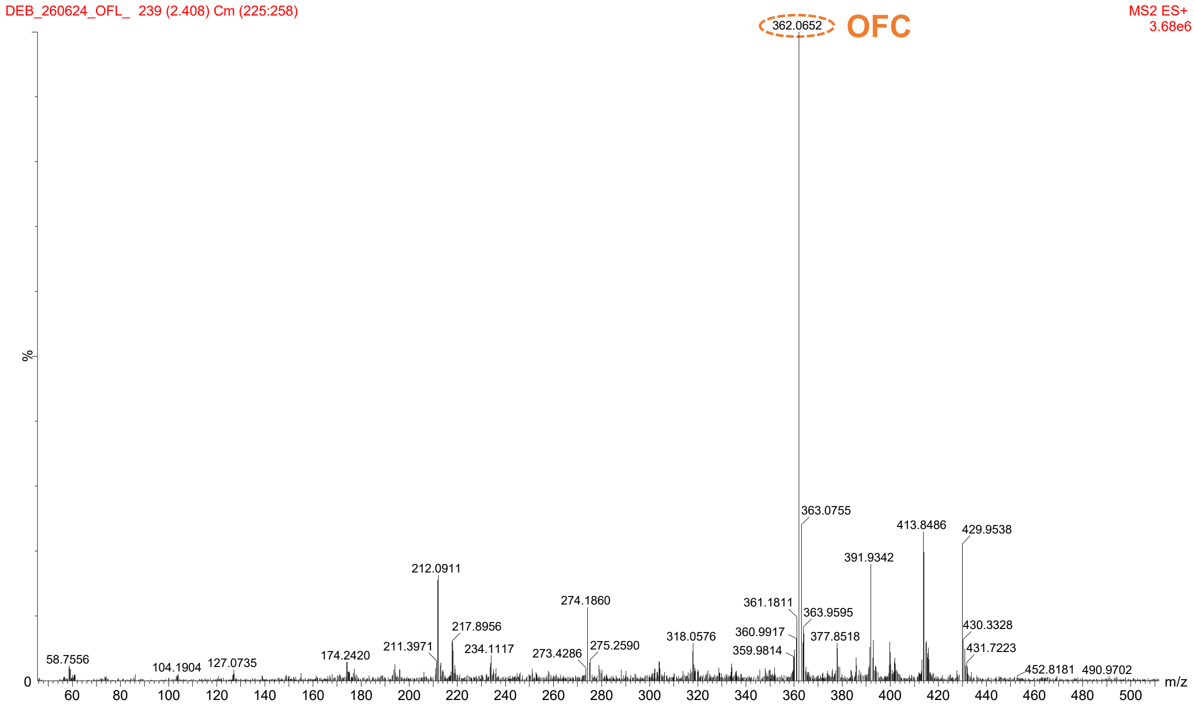
DEB_260624_OFL_ 239 (2.408) Cm (225:258)
MS2 ES+
3.68e6
362.0652
OFC
%
363.0755
413.8486
429.9538
391.9342
212.0911
274.1860
361.1811
363.9595
430.3328
217.8956
360.9917
377.8518
211.3971
234.1117
275.2590
318.0576
431.7223
58.7556
104.1904
127.0735
174.2420
273.4286
359.9814
452.8181
490.9702
m/z

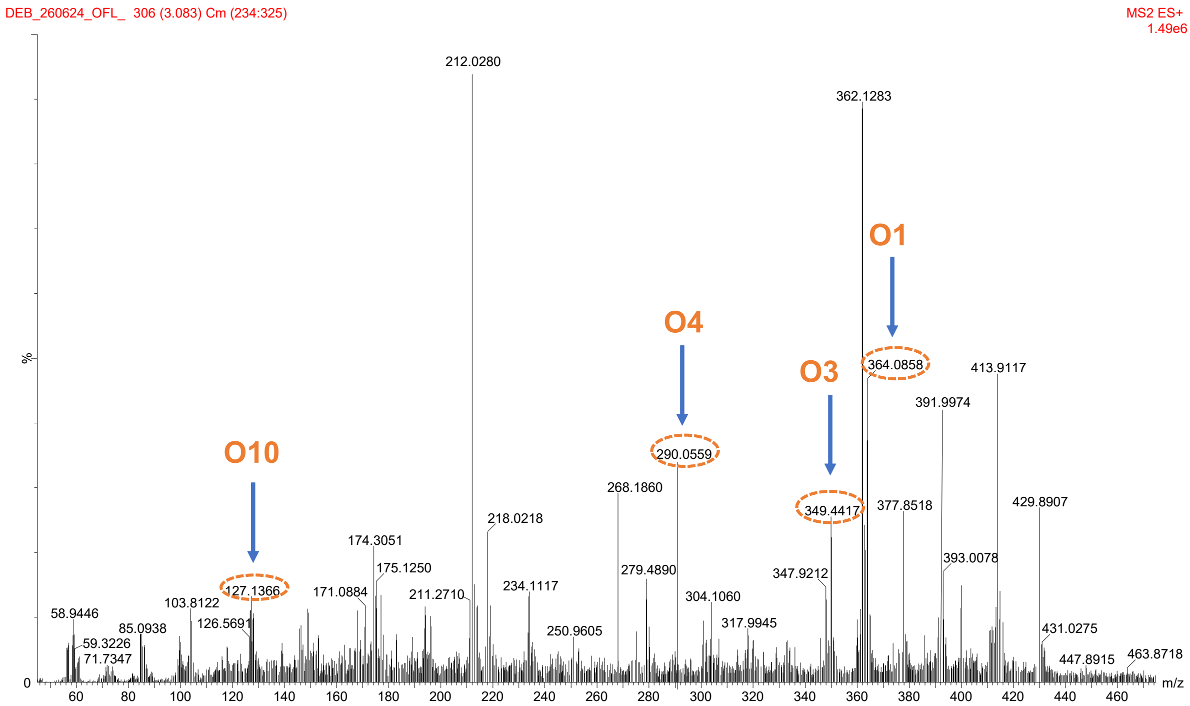
DEB_260624_OFL_ 306 (3.083) Cm (234:325)
MS2 ES+
1.49e6
212.0280
362.1283
O1
O4
O3
364.0858
413.9117
%
391.9974
O10
290.0559
268.1860
349.4417
377.8518
429.8907
218.0218
174.3051
393.0078
175.1250
279.4890
347.9212
127.1366
171.0884
211.2710
234.1117
304.1060
58.9446
103.8122
126.5691
317.9945
85.0938
250.9605
431.0275
59.3226
71.7347
447.8915
463.8718
m/z

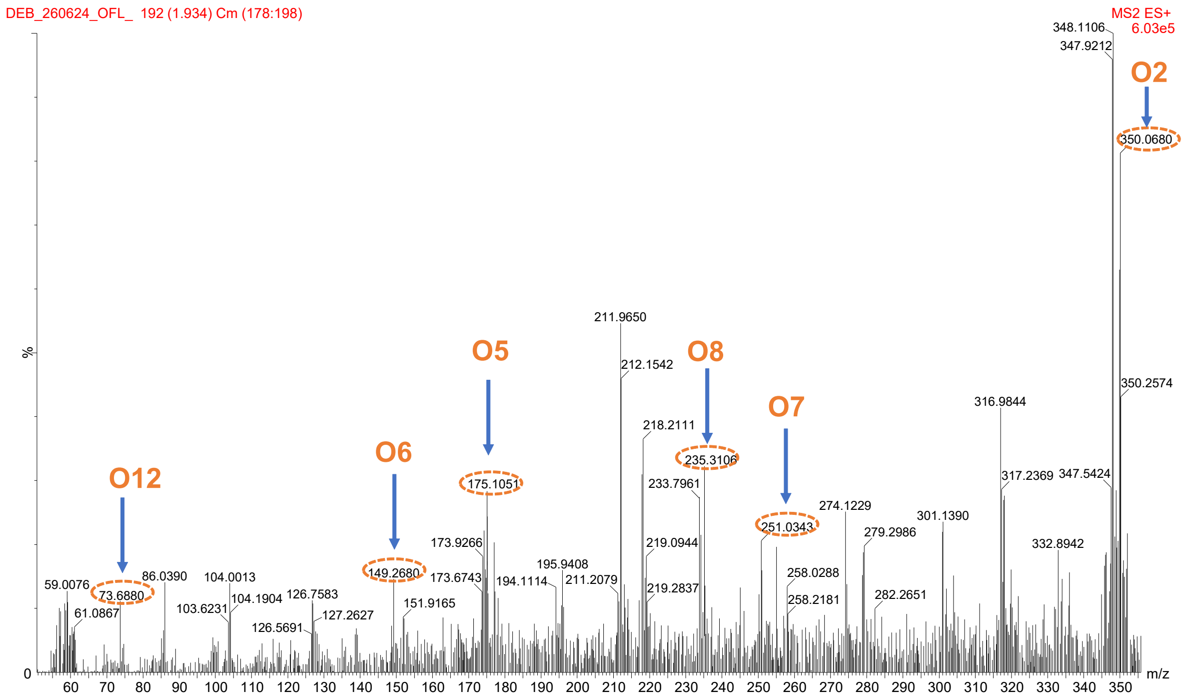
DEB_260624_OFL_ 192 (1.934) Cm (178:198)
MS2 ES+
6.03e5
O2
O5
O6
O8
O7
O12
348.1106
347.9212
350.0680
350.2574
211.9650
212.1542
218.2111
235.3106
233.7961
175.1051
173.9266
149.2680
251.0343
274.1229
279.2986
301.1390
316.9844
317.2369
347.5424
332.8942
73.6880
m/z

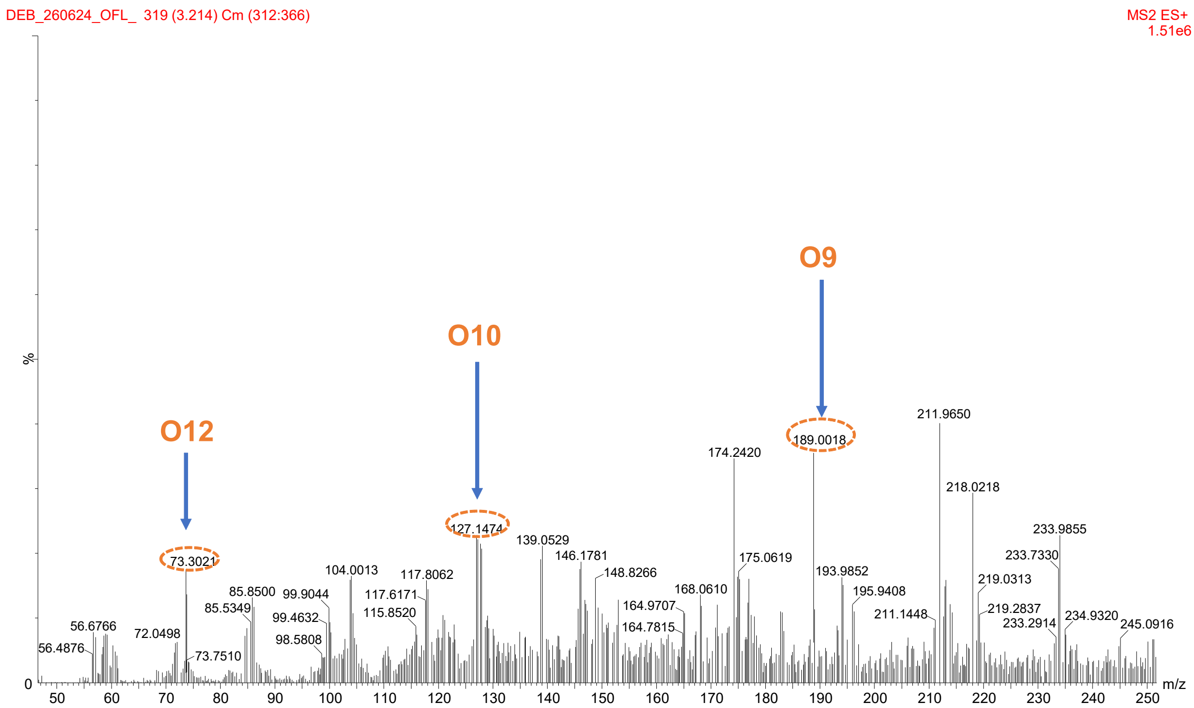
DEB_260624_OFL_ 319 (3.214) Cm (312:366)
MS2 ES+
1.51e6
O9
O10
O12
189.0018
127.1474
73.3021
211.9650
174.2420
218.0218
233.9855
m/z

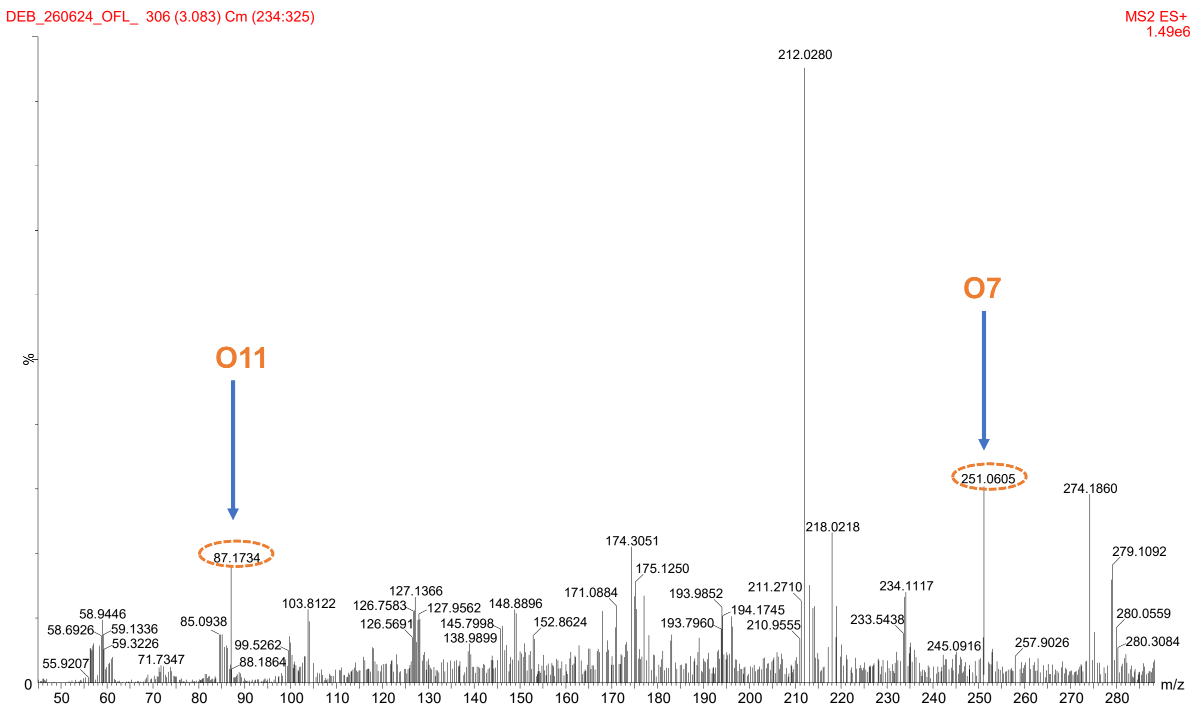

Fig. S5. LCMS spectra of OFC degradation products.

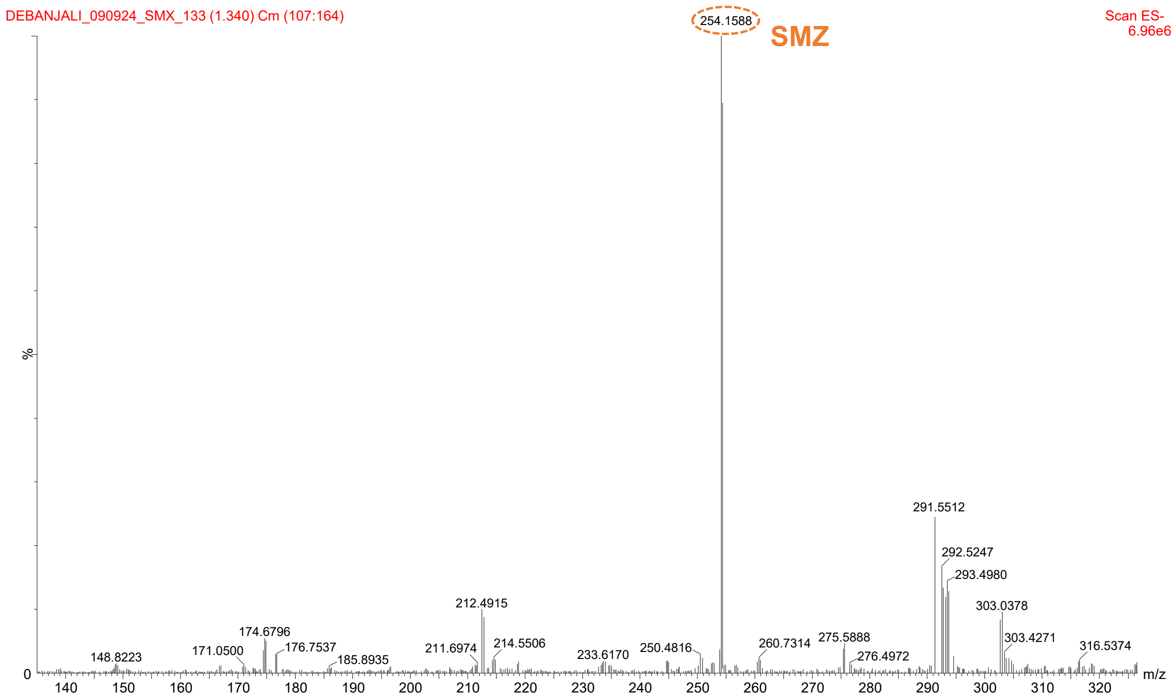
DEBANJALI_090924_SMX_133 (1.340) Cm (107:164)
Scan ES-
6.96e6
254.1588
SMZ
%
291.5512
292.5247
293.4980
303.0378
303.4271
316.5374
212.4915
174.6796
176.7537
171.0500
148.8223
185.8935
211.6974
214.5506
233.6170
250.4816
260.7314
275.5888
276.4972
m/z

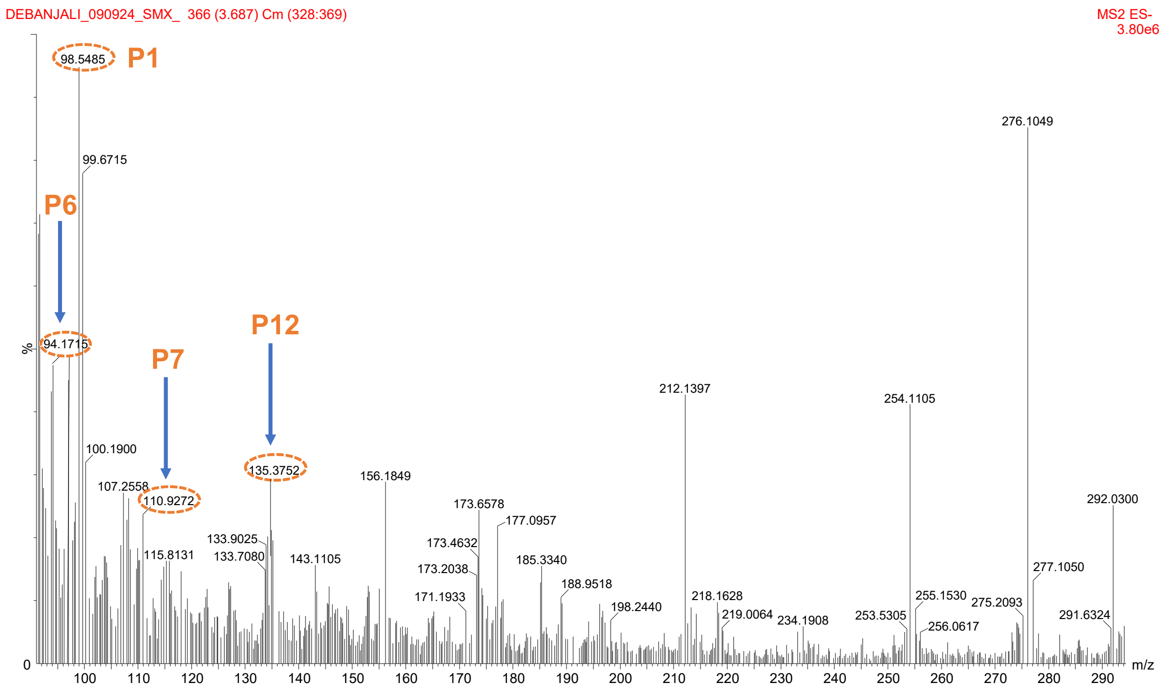
DEBANJALI_090924_SMX_ 366 (3.687) Cm (328:369)
MS2 ES-
3.80e6
98.5485
P1
99.6715
P6
94.1715
P7
P12
%
276.1049
212.1397
254.1105
100.1900
107.2558
110.9272
135.3752
156.1849
115.8131
133.9025
133.7080
143.1105
173.6578
177.0957
173.4632
173.2038
171.1933
185.3340
188.9518
198.2440
218.1628
219.0064
234.1908
253.5305
255.1530
256.0617
275.2093
277.1050
291.6324
292.0300
m/z

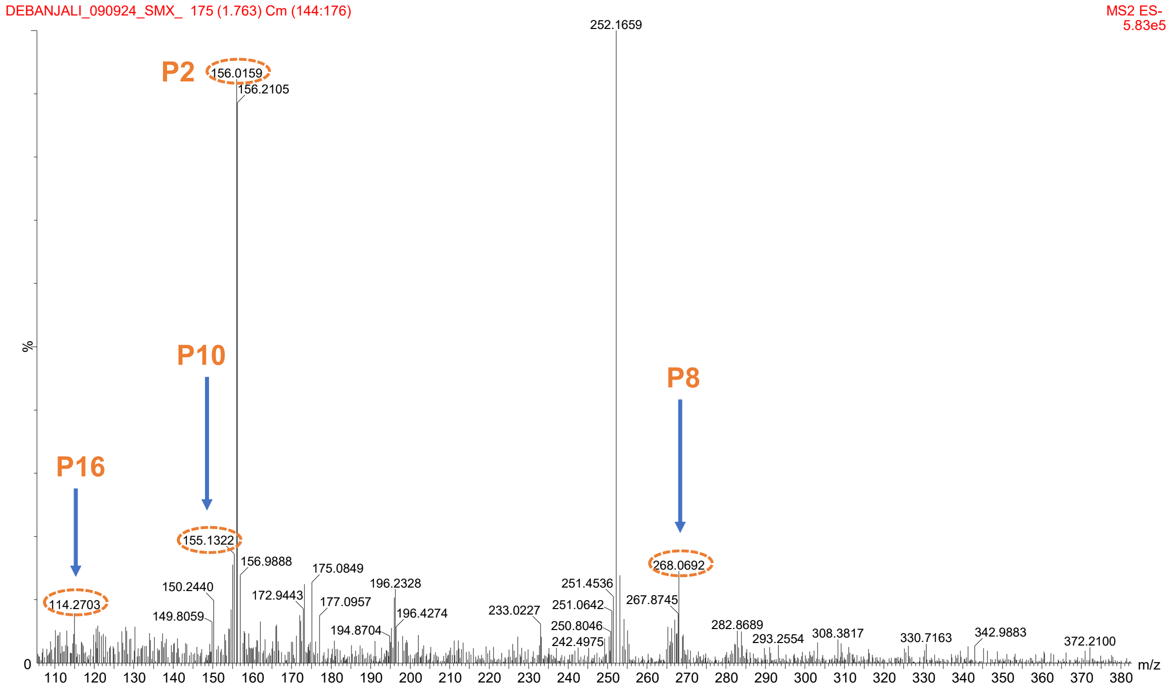

DEBANJALI_090924_SMX_ 175 (1.763) Cm (144:176)
MS2 ES-
5.83e5
252.1659
P2
156.0159
156.2105
P10
155.1322
P16
114.2703
P8
268.0692
156.9888
175.0849
150.2440
172.9443
177.0957
196.2328
196.4274
149.8059
194.8704
233.0227
251.4536
251.0642
250.8046
242.4975
267.8745
282.8689
293.2554
308.3817
330.7163
342.9883
372.2100
%
m/z

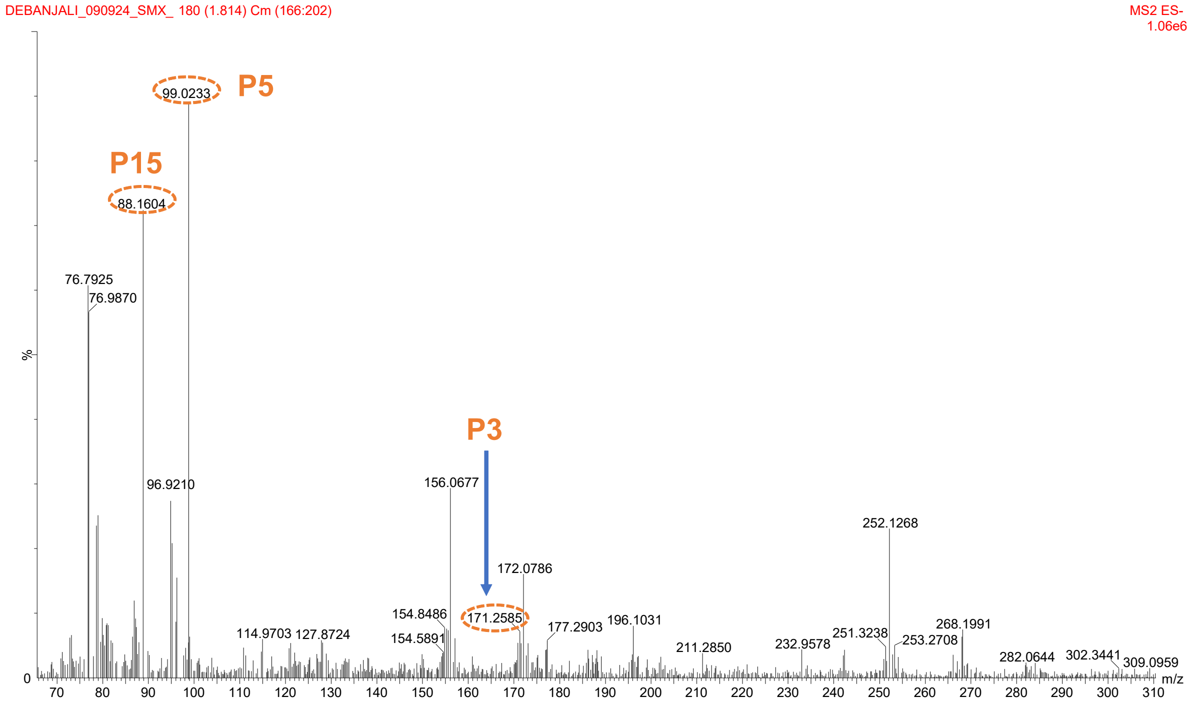

DEBANJALI_090924_SMX_ 180 (1.814) Cm (166:202)
MS2 ES-
1.06e6
P5
99.0233
P15
88.1604
76.7925
76.9870
96.9210
P3
156.0677
172.0786
154.8486
171.2585
154.5891
177.2903
196.1031
114.9703
127.8724
211.2850
232.9578
251.3238
252.1268
253.2708
268.1991
282.0644
302.3441
309.0959
%
m/z

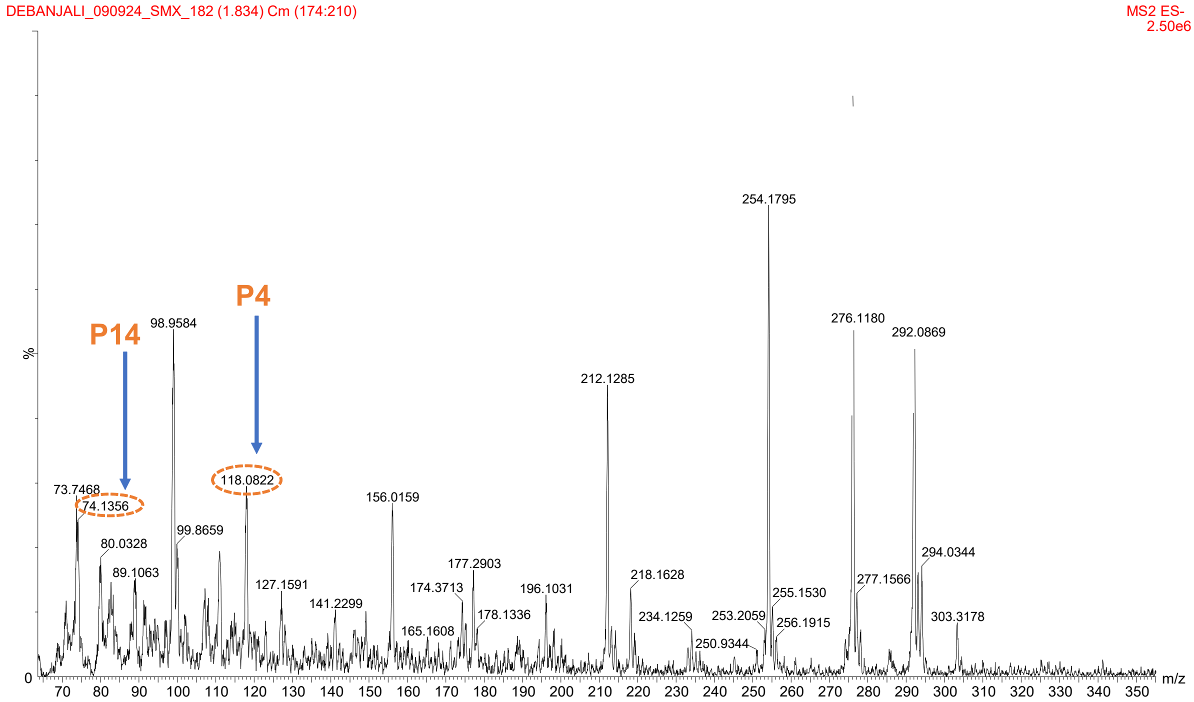

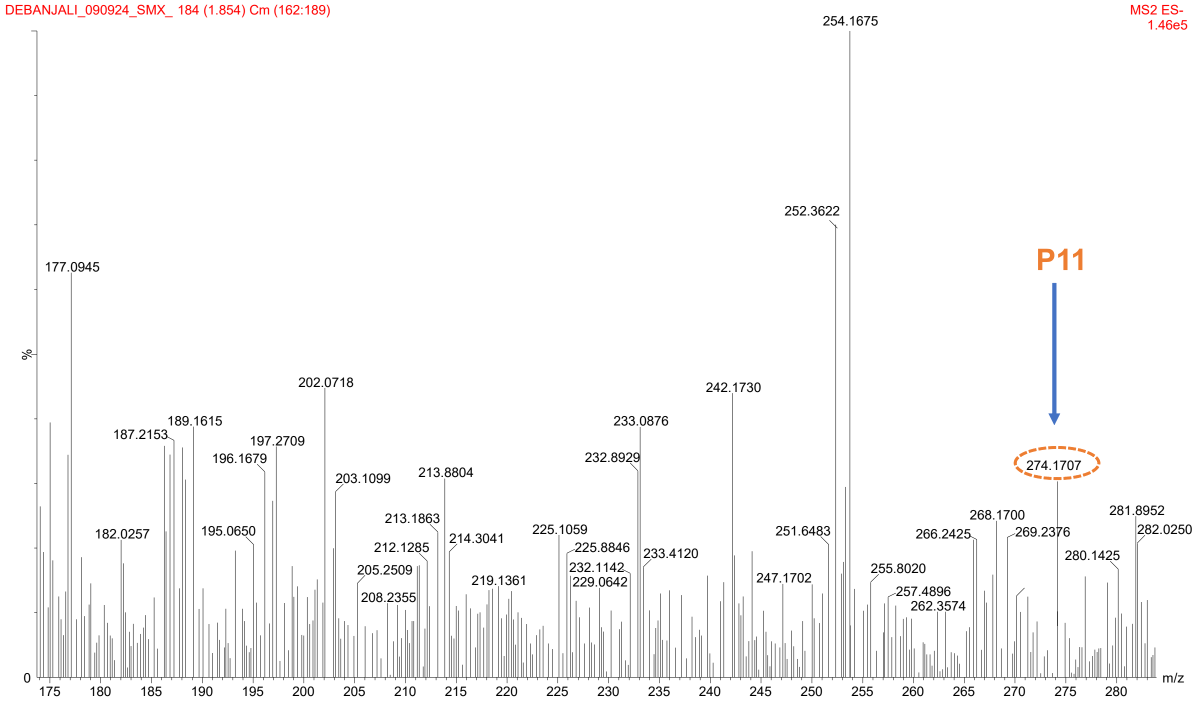

Fig. S6. LCMS spectra of SMZ degradation products.

Table S1: Elemental composition of various non-metal-doped GCN samples, as determined by XPS.

Sample	C (at.%)	N (at.%)	O (at.%)	F (at.%)	B (at.%)	S (at.%)	P (at.%)
B-GCN	51.15	36.19	9.85	–	2.81	–	–
S-GCN	50.53	40.55	7.10	–	–	1.82	–
P-GCN	51.6	38.07	7.8	–	–	–	2.53
F-GCN	47.74	41.53	8.32	2.41	–	–	–

Table S2: Textural properties of pristine GCN and its non-metal-doped variants.

Sample	Specific surface area (m^2 g^{-1})	Pore volume (cm^3 g^{-1})	Average pore diameter (nm)
GCN	6.0	0.052	29.07
B-GCN	5.3	0.058	48.69
S-GCN	6.7	0.059	40.50
P-GCN	7.4	0.066	41.92
F-GCN	13	0.102	35.31

Table S3. Comparison of the antibiotic degradation performance of F-GCN with previously reported semiconductor-based photocatalytic systems.

Photocatalyst	Antibiotic	Conc. (mg L^{-1})	Reaction time (min)	Degradation (%)	Degradation rate constant (min^{-1})	TOC removal (%)	Reference
$MnWO_4$/g-C_3N_4	OFC	10	70	90.4	3.3×10^{-2}	–	1
30%$Gd_2Ti_2O_7$/SiO_2	OFC	10	90	79.1	1.7×10^{-2}	–	2
BiOCl/TiO_2	OFC	200	10	70	2.6×10^{-1}	80 in 2 h	3
MnFeCoNiCu NPs	OFC	5	120	94	21×10^{-3}	74	4
CdS/TiO_2	OFC	10	180	86	8.9×10^{-3}	48.5 in 270 min	5
2S–Bi_2O_3/MnO_2	SMZ	5	240	86.1	7.3×10^{-3}	59.5	6
ZnO/$ZnIn_2S_4$	SMZ	2.5	390	74.9	3.6×10^{-3}	41.49 in 6.5 h	7
BCN/GA	SMZ	5	120	93.7	1.7×10^{-2}	–	8
2%P-g-C_3N_4	SMZ	10	180	70	–	–	9
g-C_3N_4@PDA/BiOBr	SMZ	2.5	60	71	–	60 in 180 min	10
F-GCN	OFC, SMZ	10	90	98.9	5.8×10^{-2}	82.3	This study
F-GCN	SMZ	10	90	96.6	3.6×10^{-2}	78.5	This study

Text S1:

It is evident from Table S2 that the degradation rate constants of F-GCN (5.8×10^{-2} min^{-1} for OFC and 3.6×10^{-2} min^{-1} for SMZ) are notably higher than those of most reported photocatalysts. Consequently, F-GCN achieves high efficiency within 90 min, whereas many other systems require longer times and achieve lower degradation. Beyond kinetics, F-GCN also excels in overall photocatalytic performance. Its mineralization efficiency reaches nearly 80%, surpassing most systems that primarily achieve only partial degradation (Table S2). In addition, F-GCN retains over 90% of its activity after three consecutive cycles, demonstrating excellent durability. Another important advantage is its stable performance across a wide pH range (pH 3–9), whereas several reported photocatalysts show sharp decreases in activity outside neutral conditions. Collectively, these features, including high degradation and mineralization efficiencies, reusability, and broad pH tolerance, underscore the practical applicability of F-GCN beyond simple numerical rate comparisons.

Table S4: Water quality parameters of the various real water matrices analysed according to APHA 23rd Ed.

Parameters	**Unit**	**TW**	**RW**	**MWW**	**HWW**
pH	_	7.03	6.6	5.8	6.2
Turbidity	NTU	<1	<1	2.8	12.5
Total dissolved solid (TDS)	mg L^{-1}	186	173.8	386.2	434.6
Total suspended solid (TSS)	mg L^{-1}	< 5	3.2	9.8	44.8
Chemical oxygen demand (COD)	mg L^{-1}	< 4	20	80	30
Biological oxygen demand (BOD)	mg L^{-1}	< 2	6.6	22.6	13.7
Phosphate (PO_4^{3-})	mg L^{-1}	0.65	<0.05	1.9	7.6
Sulfate (SO_4^{2-})	mg L^{-1}	3.5	11.52	26.6	12.1
Nitrate (NO_3^{-})	mg L^{-1}	2.9	0.19	17.4	8.7
Chloride (Cl^{-})	mg L^{-1}	21.9	25.7	71.6	69.5
Carbonate (CO_3^{2-}) as $CaCO_3$	mg L^{-1}	71.4	90.3	140.6	197.9

Table S5: Viable colony-forming units (CFU) per mL for OFC and SMZ before and after photocatalytic treatment with F-GCN, with deionized water as the control.

Pollutant		**CFU mL^{-1} (mean ± SD)**
OFC	Control	$(83.7 \pm 6) \times 10^7$
	Untreated	$(6 \pm 3.6) \times 10^7$
	Treated	$(91.3 \pm 5) \times 10^7$
SMZ	Control	$(84 \pm 7) \times 10^7$
	Untreated	$(3.7 \pm 2.1) \times 10^7$
	Treated	$(74.7 \pm 7) \times 10^7$

Table S6: Germination percentage, root length, and shoot length of *Vigna radiata* seedlings treated with different water samples.

Sample		Germination (%)	Average shoot length (cm)	Average root length (cm)
OFC	Deionized water	74 ± 3.1	3.72 ± 0.21	2.54 ± 0.13
	Untreated	27 ± 2.3	2.17 ± 0.09	0.87 ± 0.08
	Treated	67 ± 2.8	4.18 ± 0.18	1.78 ± 0.1
SMZ	Deionized water	80 ± 3.4	4.84 ± 0.15	1.87 ± 0.16
	Untreated	34 ± 1.9	1.8 ± 0.10	0.43 ± 0.1
	Treated	74 ± 2.5	3.64 ± 0.20	1.44 ± 0.12

References

(1) S.L. Prabavathi, K. Saravanakumar, G. Mamba, V. Muthuraj, 1D/2D $MnWO_4$ nanorods anchored on g-C_3N_4 nanosheets for enhanced photocatalytic degradation ofloxacin under visible light irradiation, *Colloids Surf A Physicochem Eng Asp,* 2019, *581*, 123845. https://doi.org/10.1016/j.colsurfa.2019.123845.

(2) W. Zhang, Y. Liu, C. Li, Photocatalytic degradation of ofloxacin on $Gd_2Ti_2O_7$ supported on quartz spheres, *J Phys Chem Solids,* 2018, *118*, 144–149. https://doi.org/10.1016/j.jpcs.2018.03.019.

(3) Q. Wang, P. Li, Z. Zhang, C. Jiang, K. Zuojiao, J. Liu, Y. Wang, Kinetics and mechanism insights into the photodegradation of tetracycline hydrochloride and ofloxacin mixed antibiotics with the flower-like BiOCl/TiO_2 heterojunction, *J Photochem Photobiol A Chem,* 2019, *378*, 114–124. https://doi.org/10.1016/j.jphotochem.2019.04.028.

(4) S. Das, M. Sanjay, S. Kumar, S. Sarkar, C.S. Tiwary, S. Chowdhury, Magnetically separable MnFeCoNiCu-based high entropy alloy nanoparticles for photocatalytic oxidation of antibiotic cocktails in different aqueous matrices, *Chem Eng J,* 2023, *476*, 146719. https://doi.org/10.1016/j.cej.2023.146719.

(5) A. Kaur, A. Umar, W.A. Anderson, S.K. Kansal, Facile synthesis of CdS/TiO_2 nanocomposite and their catalytic activity for ofloxacin degradation under visible illumination, *J Photochem Photobiol A Chem,* 2018, *360*, 34–43. https://doi.org/10.1016/j.jphotochem.2018.04.021.

(6) V. K. Parida, S. K. Srivastava, S. Chowdhury, A.K. Gupta, Visible light-assisted degradation of sulfamethoxazole on 2D/0D sulfur-doped Bi_2O_3/MnO_2 Z-Scheme heterojunction immobilized photocatalysts, *Langmui,r* 2023, *39*, 18846–18865. https://doi.org/10.1021/acs.langmuir.3c02733.

(7) X. Gan, Y. Song, G. Liu, H. Zhang, J. Yang, The efficient degradation and mechanism of sulfamethoxazole using ZnO/$ZnIn_2S_4$ heterojunction under visible light, *Front Environ Sci,* 2023, *11*. https://doi.org/10.3389/fenvs.2023.1314536.

(8) T. Shafi, C. Das, M. Naushad, B.K. Dubey, S. Chowdhury, Facile stitching of boron-doped polymeric carbon nitride with graphene-based nanosheets into a self-supporting and recoverable photocatalyst for efficient antibiotic removal from wastewater, *ACS ES&T Water,* 2025, *5*, 2268-2282. https://doi.org/10.1021/acsestwater.4c01179

(9) R. Tsolele, O.A. Arotiba, S.P. Malinga, Fabrication of phosphorus-doped graphitic carbonitride towards the photodegradation of ciprofloxacin and sulfamethoxazole, *Int J Environ Sci Technol,* 2024, *21*, 7009–7023. https://doi.org/10.1007/s13762-024-05488-w.

(10) F. Guo, J. Chen, J. Zhao, Z. Chen, D. Xia, Z. Zhan, Q. Wang, Z-Scheme heterojunction g-C_3N_4@PDA/BiOBr with biomimetic polydopamine as electron transfer mediators for enhanced visible-light driven degradation of sulfamethoxazole, *Chem Eng J,* 2020, *386*, 124014. https://doi.org/10.1016/j.cej.2020.124014.